Mechanisms of efficiency enhancement by a tapered waveguide in gyrotron backward wave oscillators

C. S. Kou, C. H. Chen, and T. J. Wu
Department of Physics, National Tsing Hua University, Hsinchu, Taiwan
(Received 3 November 1997)

The performance of a gyrotron backward wave oscillator (gyro-BWO), composed of a uniform waveguide section and a down-tapered waveguide section, is studied by a large-signal self-consistent model. Results show that the efficiency can be drastically enhanced to be 2.5 times higher than that of the gyro-BWO without tapering. Explorations of the physical mechanisms responsible for this enhancement reveal that the effects of the tapered section are twofold. First, the oscillation frequency becomes higher in the tapered case, leading to a higher initial resonance mismatch. As a result, electrons can be bunched deeper in the phase space so that most electrons can be located in the losing energy phase. Second, the reduction of the waveguide radius along the interaction region results in a growth of the coupling between the electron beam and the wave in the region where the wave power decays. In addition, the vulnerability of the efficiency to the velocity spread of the electron beam can be significantly alleviated for the wave of low oscillation frequency by using the tapered waveguide. [S1063-651X(98)00606-0]

PACS number(s): 41.60.−m, 84.40.Fe

I. INTRODUCTION

The gyrotron backward wave oscillator (gyro-BWO) is based on the electron cyclotron resonance between a backward waveguide mode and a forward electron beam. The major attractive feature of the gyro-BWO is its frequency tunability, which can be achieved by adjusting the magnetic field or beam voltage. However, the efficiency of the gyro-BWO is relatively lower than that of other gyrotron devices. The main reason for this drawback is its spatial distribution of the wave power that reaches a maximum near the entrance of the electron beam and decays along the propagation direction of electrons. This power profile leads to an earlier overbunching of electrons and a weak coupling between the wave and the electron beam.

A number of theoretical [1–7] and experimental [8–14] studies of the gyro-BWO have been reported. In Ref. [5], the efficiency of the gyro-BWO has been found to be significantly improved by tapering the magnetic field. Results found in Ref. [6] revealed that the magnetic field tapering with a positive gradient tended to increase the initial frequency mismatch leading to the efficiency enhancement. In Ref. [11], a tapered interaction structure was proposed and used in the experiment, which reported an output power of a factor of 2 higher than that of the uniform tube. Later, a comprehensive large signal theory has been developed by Nusinovich and Dumbrajs [7], which can be used to analyze the gyro-BWO with a tapered magnetic field and waveguide wall radius. It has been found in that study that the maximum orbital efficiency of the gyro-BWO with linearly tapered parameters was almost three times higher than that of the gyro-BWO without tapering. Meanwhile, the optimal tapering parameters were fully investigated to improve the efficiency.

The purpose of this study is not only to characterize the performance but also to unravel the physical mechanisms responsible for the efficiency enhancement of the gyro-BWO by a down-tapered waveguide. In this study, analyses are performed by a large-signal self-consistent model, which is similar to that used in Ref. [5] except for different expressions. As will be shown below, the upshift of the resonance frequency and the increased coupling between the electron beam and the wave caused by the down-tapered waveguide can drastically enhance the efficiency of the gyro-BWO. However, the optimization on the performance of a tapered gyro-BWO is not included in this study, which has already been fully addressed in Ref. [7].

II. THEORETICAL MODEL

The self-consistent large-signal model of the gyro-BWO is adopted from that of the gyrotron traveling-wave tube except for different operating conditions and boundary conditions. The theoretical model consists of equations for calculating the spatial evolution of the wave and the dynamics of electrons in the interaction between the wave and the electrons. In this study, the spatial variation of the waveguide radius is included. The procedure of the derivation is similar to that used in Refs. [15,16] and is briefly described in the following.

We consider an electron beam traveling through a cylindrical waveguide. An external dc magnetic field is applied in the z direction to guide the electron beam. The radius r_w of the waveguide is a slowly varying function of the position in the z direction. The electric and magnetic fields of a circularly polarized TE_{mn} waveguide mode can be expressed as

$$B_z = f(z) J_m(k_{mn} r) \exp[-i(\omega t - m\theta)],$$

$$E_r = -\frac{\omega m}{c r k_{mn}^2} f(z) J_m(k_{mn} r) \exp[-i(\omega t - m\theta)],$$

$$E_\theta = -\frac{i\omega}{c k_{mn}} f(z) J_m'(k_{mn} r) \exp[-i(\omega t - m\theta)], \qquad (1)$$

$$B_r=\frac{1}{k_{mn}}\frac{df(z)}{dz}J'_m(k_{mn}r)\exp[-i(\omega t-m\theta)],$$

$$B_\theta=\frac{im}{rk_{mn}^2}\frac{df(z)}{dz}J_m(k_{mn}r)\exp[-i(\omega t-m\theta)],$$

where $k_{mn}=x_{mn}/r_w(z)$ and x_{mn} is the nth root of $J'_m(x)=0$.

The electron dynamics are determined by the Lorentz force, given by

$$\frac{d\vec{p}}{dt}=-e\left[\vec{E}+\frac{\vec{p}}{\gamma mc}\times(\vec{B}+\vec{B}_{\rm ext})\right],$$

where $\vec{E}$ and $\vec{B}$ are the electric and magnetic fields of the wave and $B_{\rm ext}$ represents the external magnetic field, which must satisfy $\vec{\nabla}\cdot\vec{B}_{\rm ext}=0$ and can be expressed as

$$\vec{B}_{\rm ext}=B_e(z)e_z-\frac{1}{2}\frac{\partial B_e}{\partial z}re_r. \tag{2}$$

By substituting Eq. (1) for E and B of the wave and Eq. (2) into the equation of motion of the electron and following the procedure used in Refs. [15,16], a set of slow-time scaled equations governing the momentum and the phase angle of each electron can be obtained:

$$\frac{dp_z}{dz}=\frac{ep_\perp}{cp_zk_{mn}}J_{s-m}(k_{mn}r_c)J'_s(k_{mn}r_L)[F'(z)\cos\Lambda-F(z)\Phi'(z)\sin\Lambda]-\frac{ep_\perp}{2cp_z}r_L\frac{\partial B_e}{\partial z},$$

$$\frac{dp_\perp}{dz}=\frac{\gamma m_e e}{cp_zk_{mn}}J_{s-m}(k_{mn}r_c)J'_s(k_{mn}r_L)\times\left[\frac{p_z}{m_e\gamma}\frac{dF(z)}{dz}\cos\Lambda-\left(\frac{p_z}{m_e\gamma}-\omega\right)\times F(z)\frac{d\Phi(z)}{dz}\sin\Lambda\right]+\frac{1}{2}\frac{er_L}{c}\frac{\partial B_e}{\partial z}, \tag{3}$$

$$\frac{d\Lambda}{dz}=\frac{\omega\gamma m_e}{p_z}+\frac{d\Phi(z)}{dz}-s\left\{\frac{m_e\Omega_e}{p_z}+\frac{\gamma m_e e}{p_zp_\perp}J_{s-m}(k_{mn}r_c)J'_s(k_{mn}r_L)\times\left[\left(\frac{-\omega s}{k_{mn}^2cr_L}+\frac{-p_zs}{\gamma m_eck_{mn}^2r_L}\frac{d\Phi(z)}{dz}+\frac{p_\perp}{\gamma m_ec}\right)\times F(z)\cos\Lambda-\frac{p_zs}{\gamma m_eck_{mn}^2r_L}\frac{dF(z)}{dz}\sin\Lambda\right]\right\},$$

where $\Lambda(z)=\omega t-s\phi+(m-s/2)\pi+(s-m)\varphi+\Phi(z)$ and r_c and r_L are the guiding center radius and the electron Larmor radius. In deriving the above equation it has been assumed that $f(z)=F(z)\exp[-i\Phi(z)]$. Furthermore, the operating conditions are adjusted such that the sth cyclotron harmonic interaction becomes dominant.

In addition to the Lorentz force, it is also useful to include the energy change equation for checking the accuracy of numerical calculations. It is given by

$$\frac{d\gamma}{dz}=\frac{e}{m_ec^3}\frac{p_\perp}{p_z}\frac{\omega F(z)}{k_{mn}}J_{s-m}(k_{mn}r_c)J'_s(k_{mn}r_L)\sin\Lambda. \tag{4}$$

The circuit equations that govern the spatial rate of change of the wave's amplitude and phase of a waveguide mode can also be derived from Maxwell's equation, which is given by

$$\nabla^2\vec{B}-\frac{1}{c^2}\frac{\partial^2}{\partial t^2}\vec{B}=-\frac{4\pi}{c}\vec{\nabla}\times\vec{\tilde{J}}, \tag{5}$$

where $\vec{B}$ is the wave's magnetic field and $\vec{\tilde{J}}$ is the current. Taking the z component of Eq. (5) and substituting Eq. (1) for B_z, the circuit equation can be obtained, which yields

$$\left[\left(\frac{\omega^2}{c^2}-k_{mn}^2\right)F(z)+F''(z)-F(z)\Phi'^2(z)+i[-2F'(z)\Phi'(z)-\Phi''(z)F(z)]\right]=\frac{8\pi}{cC_{mn}}\int ds\langle\tilde{J}_\perp J_{s-m}(k_{mn}r_c)J'_s(k_{mn}r_L)\exp(i\Lambda)\rangle. \tag{6}$$

In the above equation, $\tilde{J}_\perp$ is the transverse current corresponding to the rotational motion of the electron, $C_{mn}=\pi r_w^2J_m^2(x_{mn})[1-m^2/x_{mn}^2]$, and the term in angular brackets is defined by

$$\langle f\rangle=\frac{1}{2\pi}\int_0^{2\pi}f\,d\Lambda_0. \tag{7}$$

The power flow can be evaluated by the Poynting vector and is given by

$$\vec{P}_w(z)=\frac{c}{8\pi}\oint ds\,\vec{E}\times\vec{H}^*=\frac{\omega C_{mn}}{8k_{mn}^2}|F(z)|^2\frac{d\vec{\Phi}}{dz}. \tag{8}$$

The energy exchange between the electron beam and the wave at each position is given by

$$\frac{dP_{\rm ex}}{dz}={\rm Re}\left\{-\int ds\,\vec{\tilde{J}}_\perp\cdot\vec{E}_\perp^*\right\}={\rm Re}\left\{-f^*(z)\int ds\,\vec{\tilde{J}}_\perp\cdot\vec{e}_\perp^*\right\}, \tag{9}$$

where $\vec{e}_\perp^*$ is the unit transverse electric field. As pointed out in Ref. [17], the induced current resulting from the motion of charge between two electrodes is equal to $-J\cdot E_1$, where the J is current and E_1 is the electric field strength when the potential between the electrodes is held at 1 V. Similarly, we define J_d as the induced current on the microwave circuit by

$$J_d=-\int ds\,\vec{\tilde{J}}_\perp\cdot\vec{e}_\perp^*. \tag{10}$$

It can be shown that J_d is given by

$$J_d = i\left(\frac{x_{mn}}{r_w}\right)^2\left(\frac{\omega}{c}\right)\int ds\langle\tilde{J}_\perp J_{s-m}(k_{mn}r_c)J_s'(k_{mn}r_L)\exp(i\Lambda)\rangle. \tag{11}$$

Thus Eq. (9) can be rewritten as

$$\frac{dP_{\rm ex}}{dz} = |f^*(z)||J_d|\cos\,\theta_d. \tag{12}$$

$|J_d|$ and θ_d are indications of the coupling between the electron beam and wave. They will be used to provide physical insight into the interaction in the following analysis.

In the calculation, the current is expressed as a sum of individual electron currents and is given by

$$J = -I_0\sum_j \frac{W_j}{r_c v_{zj}}\,\delta(r_c - r_0)(\Lambda - \Lambda_j)v_j, \tag{13}$$

where I_0 is the beam current and W_j is a dimensionless weighting factor of the jth electron. The effects of the axial velocity spread of the electrons are evaluated by assuming a Gaussian distribution. It is modeled as

$$W_j = A\,\exp\left[\frac{-(p_{zj}-p_{z0})^2}{2(\Delta p_z)^2}\right]. \tag{14}$$

In the above equation A is a normalized factor and Δp_z is approximately the standard derivation of p_{zj} from the mean value p_{z0}, assuming $\Delta p_z \ll p_z$.

To obtain a steady state of the gyro-BWO interaction, the boundary conditions on each end of the interaction region must be satisfied. Those conditions are specified by requiring traveling-wave conditions on both ends of the tube. They are written as

$$df/dz = ik_0 f \quad \text{at } z=0, \tag{15}$$

$$df/dz = -ik_0 f \quad \text{at } z=L, \tag{16}$$

where $k_0 = (\omega^2/c^2 - k_{mn}^2)^{1/2}$ and L is the length of the tube.

In the numerical solution of the steady state of a gyro-BWO interaction, the oscillation frequency and output power are initially estimated. Equation (15) can then be used to determine df/dz at $z=0$. Thus the circuit equation and the dynamics of electrons are self-consistently solved by the fourth-order Runge-Kutta algorithm. Finally, the solution of f at $z=L$ is checked with Eq. (16). The correct oscillation frequency and output power can be found by any root-finding algorithm. In this study, Powell's hybrid algorithm is employed.

III. RESULTS AND DISCUSSION

As an illustration we consider an electron beam interacting with a TE_{11} waveguide mode at the first cyclotron harmonic. The beam parameters are the beam voltage $V_b = 80$ kV, the beam current $I_b = 2$ A, $\alpha(v_\perp/v_z) = 1.4$, and the guiding center radius 0.105 cm. To demonstrate the effects of using a tapered waveguide on the interaction of the gyro-BWO, comparisons are made between a gyro-BWO with a uniform waveguide and a gyro-BWO with a down-tapered waveguide as shown in Fig. 1. The uniform case is made of a cylindrical waveguide with a radius of 0.3 cm and the length is 6.5 cm. The tapered case consists of a uniform waveguide section and a negatively tapered waveguide section. The length and radius of the uniform section are 1.5 and 0.3 cm; the radius of the tapered section linearly changes from 0.3 to 0.24 cm within a length of 5 cm. The cutoff frequencies of a TE_{11} mode corresponding to the largest radius ($r_w = 0.3$ cm) and the smallest radius ($r_w = 0.24$ cm) are 29.3 and 36.6 GHz, respectively.

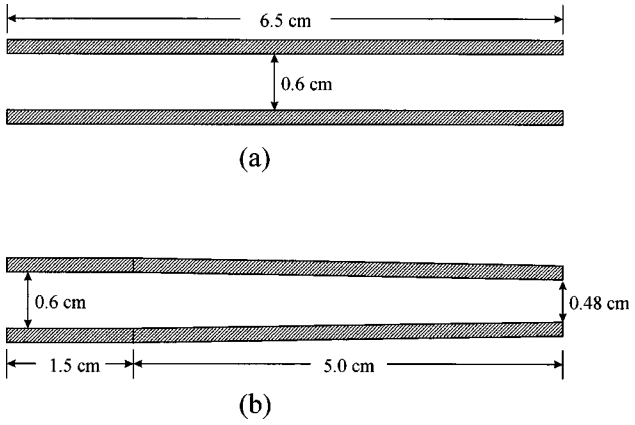

FIG. 1. Schematic of a TE_{11} mode gyro-BWO with (a) a uniform waveguide and (b) a tapered waveguide.

Figure 2 shows the output power as a function of the magnetic field in both cases. The magnetic field is expressed in the relative amplitude to the grazing magnetic field (B_g) for the waveguide radius equal to 0.3 cm, which is the magnetic field for the beam mode ($\omega - k_z v_z - s\Omega_{\rm CO}/\gamma = 0$) to be tangential to the waveguide mode ($\omega^2/c^2 - k_z^2 - k_{mn}^2 = 0$). For the uniform case, the maximum output power is 16.8 kW, corresponding to an efficiency of 10.5%. Meanwhile,

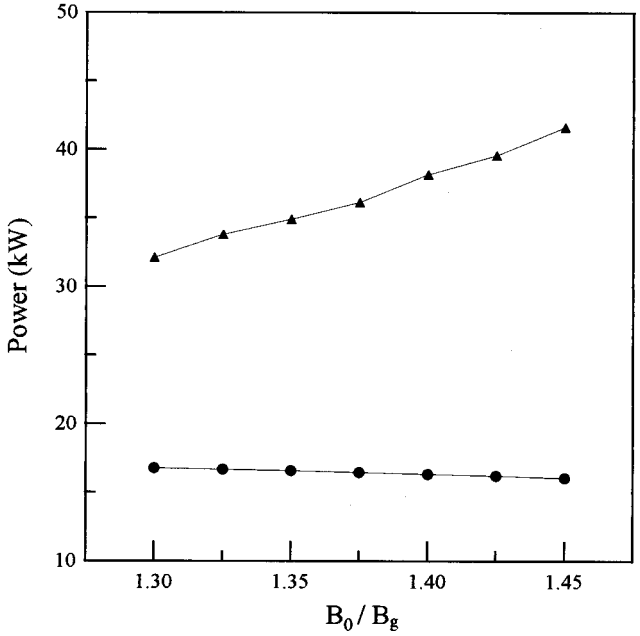

FIG. 2. Output power versus the magnetic field of a gyro-BWO with a uniform waveguide (dots) and with a tapered waveguide (triangles). The operating parameters are $V_b = 80$ kV, $I_b = 2$ A, and $\alpha = 1.4$. The dimensions of the waveguide are shown in Fig. 1.

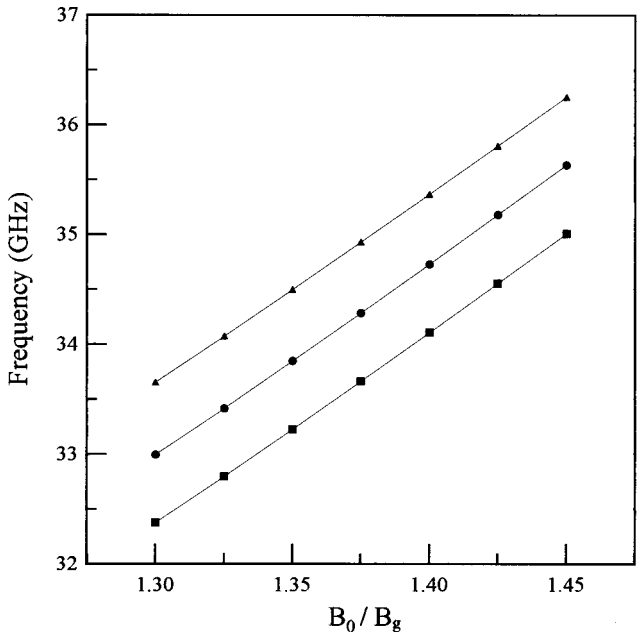

FIG. 3. Oscillation frequency as a function of the magnetic field of a gyro-BWO, with a uniform waveguide (dots) and with a tapered waveguide (triangles). The operating parameters are the same as in Fig. 2. The frequency of the intersection point between the beam mode and the waveguide mode is plotted as squares.

the output power decreases as the magnetic field is increased. It is notable that the output power has been drastically increased in the tapered case. The maximum power is 42 kW with an efficiency of 26%, which is 2.5 times higher than that of the uniform case. In contrast to that in the uniform case, the output power increases with the magnetic field. The oscillation frequency versus the magnetic field is depicted in Fig. 3. The frequency of the intersection point between the beam mode and the waveguide mode in the uniform case is also plotted. Results show that the oscillation frequency increases with the magnetic field and is higher than the frequency of the intersection point. This result is simply due to the requirement that $\omega - k_z v_z - s\Omega_{CO}/\gamma \geq 0$ for electrons to lose their energy to the wave in the gyrotron interaction. Figure 3 illustrates that the employment of a tapered section causes an oscillation frequency higher than that of the uniform case.

The physical mechanism of the efficiency enhancement by the tapered interaction structure mainly originates from the upshift of the oscillation frequency. As pointed out in Ref. [18], the electron phase shift is determined by the initial resonance mismatch, as defined by

$$\Delta = \omega + |k_z| v_z - \Omega_{CO}/\gamma,$$

where a positive sign is placed before the absolute value of the wave number because a backward wave interaction is considered. Specifically, this initial resonance mismatch determines the initial slope of the spatial evolution of the electron phase Λ. The larger the resonance mismatch, the steeper the slope. As a result, the electron can be inertially bunched deeper in the phase space. For comparisons, the electron phase trajectories of both cases for $B_0 = 1.35 B_g$ are plotted in Fig. 4. The higher ω and k_z in the tapered case lead to a

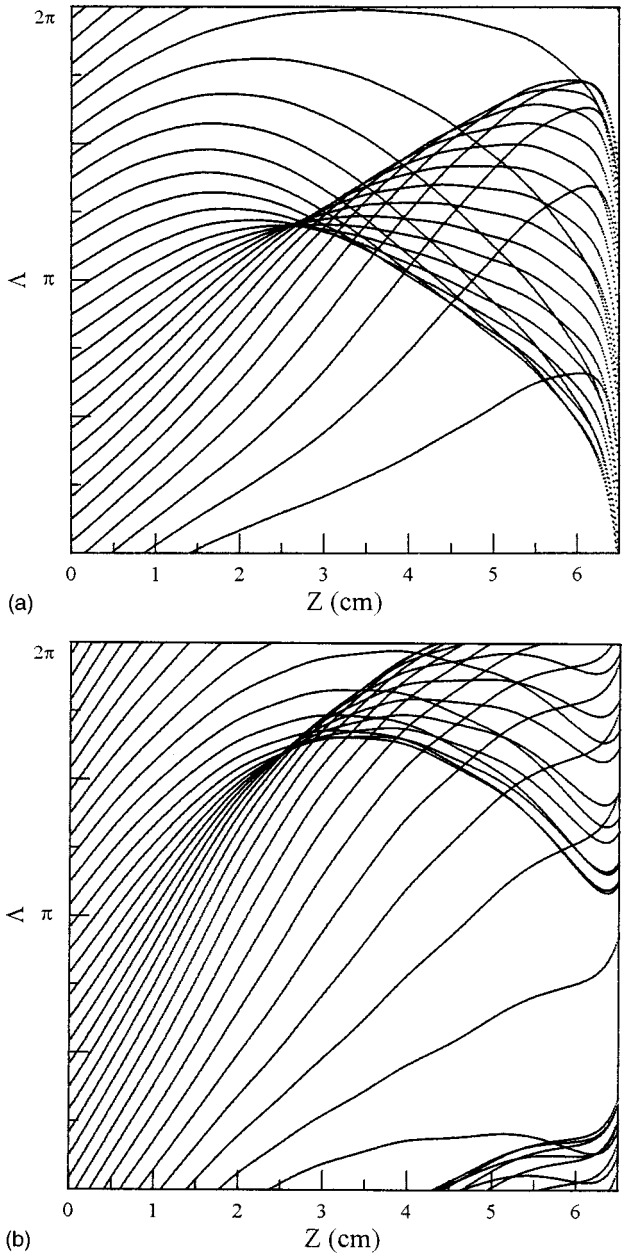

FIG. 4. Spatial evolution of electron phase trajectories of a gyro-BWO with (a) a uniform waveguide and (b) a tapered waveguide.

larger resonance mismatch so that electrons move faster in the phase space and form a compact bunch near $\Lambda = 1.7\pi$. Note that most electrons are confined in the losing energy phase throughout the interaction region after forming a compact bunch, although they expand in the phase space. On the other hand, electrons in the uniform case form a compact bunch near $\Lambda = 1.2\pi$ so that fewer electrons can remain in the losing energy phase afterward. Consequently, employing a tapered section can result in more net energy transfer from the electron beam to the wave.

In addition to a better bunching process, the down-tapered interaction section can induce further effects. Figure 5 depicts the spatial evolution of the wave power and the induced current defined by Eq. (10). In the uniform case as shown in Fig. 5(a), the power reaches a maximum near the electron beam entrance and decays in the propagation direction of the

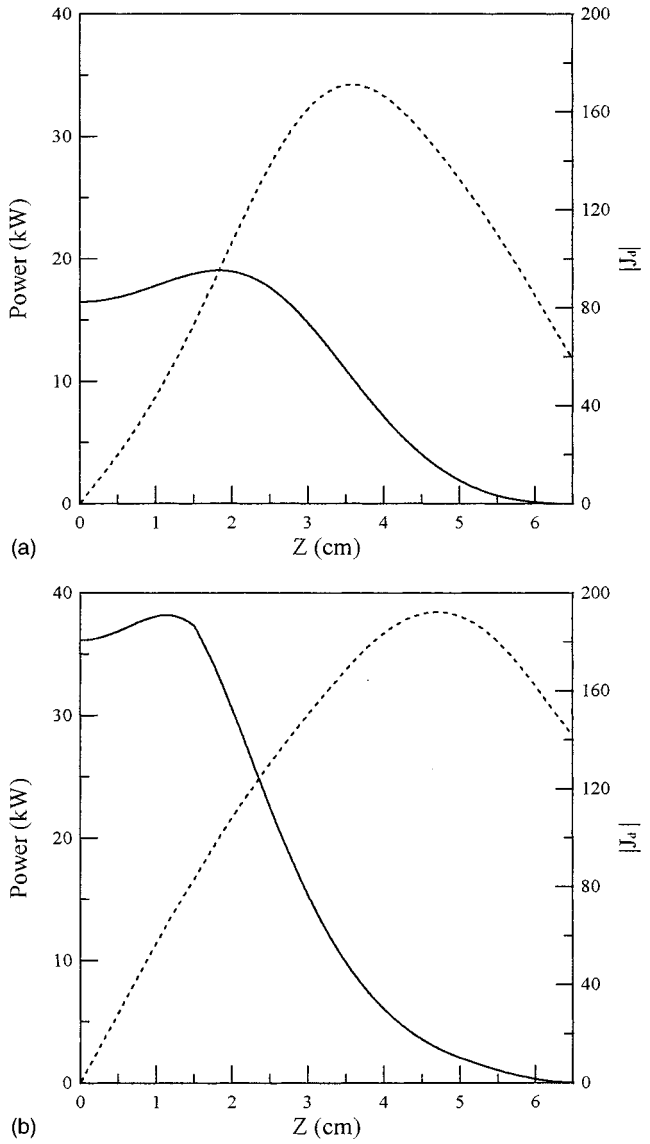

FIG. 5. Spatial evolution of the wave power (solid line) and the amplitude of the induced current J_d (dashed line) of a gyro-BWO with (a) a uniform waveguide and (b) a tapered waveguide.

electrons. As a result, electrons are strongly modulated by the wave in the beginning of the interaction region so that the electrons are quickly bunched in a shallow losing energy phase as illustrated in Fig. 4(a). Consequently, fewer electrons can transfer their energy to the wave. It is interesting to note that the induced current, representing the coupling between the electron beam and the unit transverse electric field, continues increasing after the maximum of the power and reaches a peak in a position where the wave strength actually decays. This behavior can be interpreted by the electron phase trajectories shown in Fig. 4(a), which illustrates that the electrons are compactly bunched at $z \cong 2.5$ cm while the maximum of the wave power occurs at $z \cong 1.85$ cm. Although electron phases become divergent after $z \cong 2.5$ cm, the averaged electron phase moves upward into a stronger interaction phase. Nevertheless, the induced current starts to decrease because the divergence of the electron phases becomes severe.

In the tapered case as depicted in Fig. 5(b), the power profile seems more unfavorable to the interaction because the

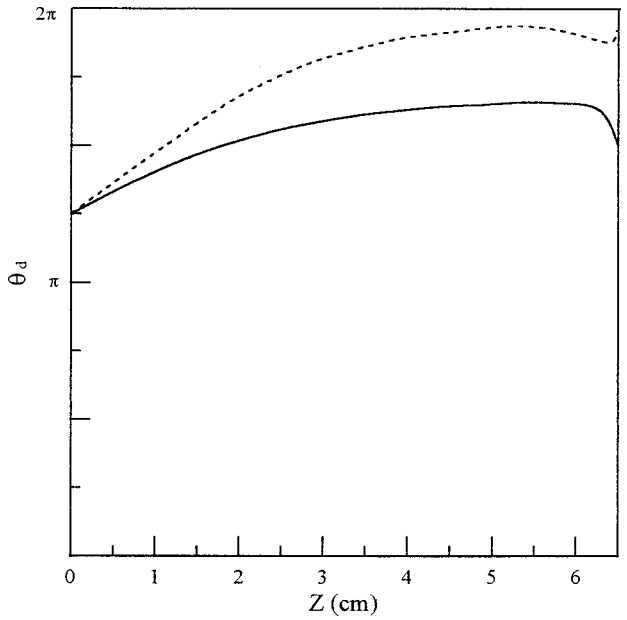

FIG. 6. Phase between the induced current and the wave as a function of position of a gyro-BWO with a uniform waveguide (solid line) and with a tapered waveguide (dashed line).

maximum of the wave power occurs earlier than that in the uniform case. Meanwhile, the electrons in the tapered case, as illustrated in Fig. 4(b), also form a compact bunch near $z \cong 2.5$ cm, which is the same as that in the uniform case. Thus it may be deduced that the induced current would start to decrease even earlier than that in the uniform case. However, the resonance mismatch in the tapered case becomes larger in the uniform waveguide section due to the upshift of the oscillation frequency, but it becomes increasingly smaller in the tapered section. Therefore, the coupling between the electron and the wave in the tapered case is made weaker in the uniform section but becomes stronger along the tapered section than that in the uniform case. Therefore, the increasing of the induced current can last longer in the tapered case. It has also been shown by Eq. (11) that the amplitude of the induced current is inversely proportional to the square of the wall radius. Consequently, more energy transfer from the electron beam to the wave in the tapered case can occur in the region where the field strength of the wave decays.

The spatial evolution of the relative phase between the wave and the induced current is depicted in Fig. 6. This phase, denoted as θ_d and defined by Eq. (12), can indicate the averaged electron phase and determines the energy exchange between the wave and the electron beam. For the uniform case (solid line), the phase starts from the gaining energy region of the electron and gradually evolves into the losing energy region. Finally, it reaches a plateau. The absorption of the wave energy by the electrons in the beginning of the interaction region causes the amplitude of the wave power on the output end to drop by $\sim 13\%$ of the maximum power, as shown in Fig. 5(a). On the other hand, the appearance of a plateau region indicates that the averaged electron phase only slightly changes. It results from the fact that the wave strength is decaying and becomes weaker in this region. Therefore, the net energy exchange between the wave and the electrons is small. For the tapered case (dashed line), the slope of the phase variation is steeper so that it quickly

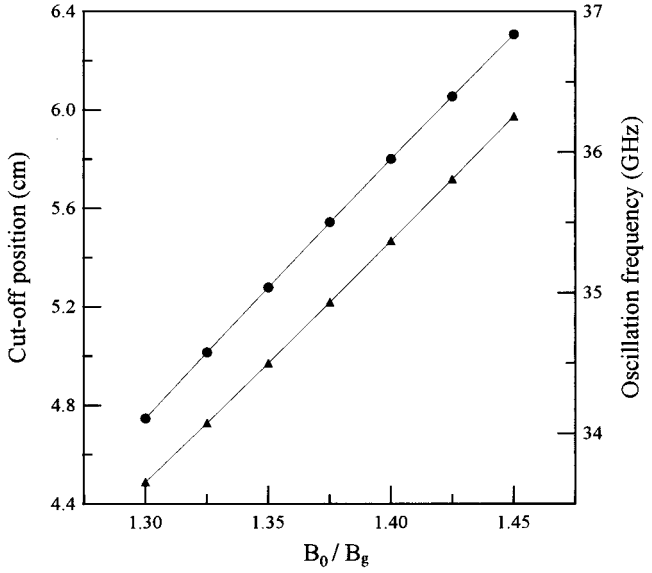

FIG. 7. Cutoff position (dots) and the associated oscillation frequency (triangles) versus the magnetic field of the gyro-BWO as shown in Fig. 1(b).

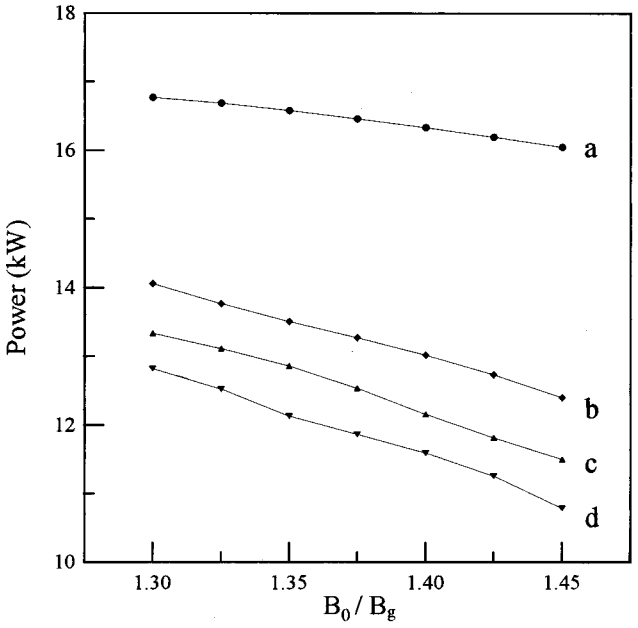

FIG. 8. Output power versus the magnetic field of a gyro-BWO with a uniform waveguide for different velocity spreads: (a) $\Delta v_z/v_z=0.0\%$, (b) $\Delta v_z/v_z=5\%$, (c) $\Delta v_z/v_z=6\%$, and (d) $\Delta v_z/v_z=7\%$.

reaches the losing energy region of the electron. Meanwhile, the initial resonance mismatch is also larger than that of the uniform case, leading to a weaker interaction. Thus the reduction of the power at the output end is less severe than that in the uniform case, as shown in Fig. 5(b). In addition, the variations of the phase from $z=1.5$ cm to the end of the tube are larger than those in the uniform case, indicating a stronger interaction induced by the down-tapered section.

Figure 2 also demonstrates different output power variations with the magnetic field in the uniform and the tapered cases. The decrease of the output power in the uniform case can be attributed to the fact that the gyrotron interaction originates from the coupling between electrons and the transverse electric fields of the waveguide mode, but the ratio between the transverse electric and magnetic fields of a TE_{mn} waveguide mode decreases with the frequency, which is defined as the wave impedance and is given by

$$Z_{TE}=\omega\mu_0/\beta,$$

where β is the propagation constant. Thus the coupling between the beam mode and the waveguide mode in the gyrotron becomes weaker when these two modes intersect at a higher frequency because the transverse electric field becomes weaker. In the contrast, the wave impedance becomes increasingly larger in the tapered waveguide section. This process occurs at each oscillation frequency and the cutoff position increases with the oscillation frequency, as depicted in Fig. 7. Moreover, most electrons are confined in the losing energy phase in the tapered waveguide section as illustrated above. Consequently, the effective interaction length becomes longer for the wave of a higher frequency. In addition, the initial resonance mismatch also increases with the oscillation frequency, which is also favored for more output power as discussed above. Due to those effects, the output power in the tapered case increases with the magnetic field.

The sensitivity of the output power to the velocity spread of the electron beam is shown in Figs. 8 and 9 for the uniform case and the tapered case, respectively. Results show that the output power at the high-frequency side is more vulnerable to the velocity spread than that at the low-frequency side. For an electron beam with a 7% velocity spread, the output power in the uniform case can be reduced by 30% at 33 GHz ($B_0=1.3B_g$), while the reduction increased to 45% at 35.6 GHz ($B_0=1.45B_g$). This characteristic is caused by the fact that the wave number is larger at

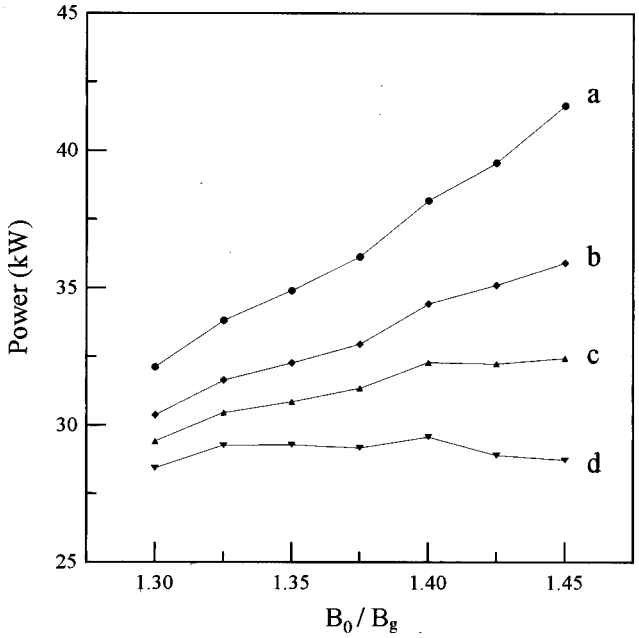

FIG. 9. Output power versus the magnetic field of a gyro-BWO with a tapered waveguide for different velocity spreads: (a) $\Delta v_z/v_z=0.0\%$, (b) $\Delta v_z/v_z=5\%$, (c) $\Delta v_z/v_z=6\%$, and (d) $\Delta v_z/v_z=7\%$.

the high-frequency side so that the velocity spread can induce more deviations in the Doppler shift term of the resonance condition. It is noticeable that the deterioration caused by the velocity spread at the low-frequency side is significantly reduced in the tapered case. For instance, for an electron beam with a 7% velocity spread at $B_0 = 1.3B_g$, the reduction of the output power by the velocity spread can be improved from 30% in the uniform case to only 5% in the tapered case. This dramatic improvement is possibly because the effective interaction length of the tapered case at the low-frequency side is much less than that of the uniform case. As shown in Fig. 8, the cutoff position for $B_0 = 1.3B_g$ is 4.75 cm, while the interaction length of the uniform case is 6.5 cm.

IV. CONCLUSION

In summary, the performance of a gyro-BWO composed of a uniform waveguide section and a tapered waveguide section is studied by a self-consistent large-signal model. The output power has been found to be significantly increased to 2.5 times higher than that of the gyro-BWO without tapering, consistent with the results of Ref. [7]. The physical mechanisms of the efficiency enhancement by using the down-tapered waveguide are twofold. First, the oscillation frequency in the tapered case is increased, resulting in a larger initial resonance mismatch. Consequently, the slope of the electron phase trajectories becomes steeper so that electrons can be bunched deeper in the phase space to get stronger interactions with the wave. Moreover, most electrons can be confined in the losing energy phase even after forming a compact bunching. Second, the reduction in the waveguide radius along the interaction region causes the coupling between the wave and the electron beam to increase when electron phase trajectories start to be divergent after compact bunching. Therefore, efficient energy transfer can still be achieved in the region where the wave strength decays. This can alleviate the unfavorable effects caused by the spatial field profile of the wave in the gyro-BWO.

The output power in the tapered case increases as the magnetic field becomes larger, while it decreases in the uniform case. This behavior may be caused by that fact that the initial resonance mismatch becomes larger at the high oscillation frequency and the effective interaction length increases with the frequency as well. Meanwhile, the sensitivity of the output power to the velocity of the electron beam has also been studied. Results show that the output power at the high-frequency side is more vulnerable to velocity spread in the uniform and the tapered cases. On the other hand, significant reduction of the detrimental effects caused by the velocity spread has been observed at the low-frequency side in the tapered case.

ACKNOWLEDGMENT

This work was sponsored by the National Science Council (Taiwan, Republic of China) under Contract No. NSC87-2112-M007-017.

[1] J. M. Wachtell and E. J. Wachtell, Appl. Phys. Lett. **37**, 1059 (1980).
[2] S. Y. Park, V. L. Granatstein, and R. K. Parker, Int. J. Electron. **57**, 1109 (1984).
[3] C. S. Kou, Phys. Plasmas **1**, 3093 (1994).
[4] M. Caplan, in *Conference Digest of the Twelfth International Conference on Infrared Millimeter Waves*, edited by R. J. Temkin (IEEE, New York, 1987), p. 276.
[5] A. K. Ganguly and S. Ahn, Int. J. Electron. **67**, 261 (1989).
[6] A. T. Lin, Phys. Rev. A **46**, 4516 (1992).
[7] Gregory S. Nusinovich and O. Dumbrajs, IEEE Trans. Plasma Sci. **24**, 620 (1996).
[8] S. Y. Park, R. H. Kyser, C. M. Armstrong, R. K. Parker, and V. L. Granatstein, IEEE Trans. Plasma Sci. **18**, 321 (1990).
[9] Thomas A. Spencer, Ronald M. Gilgenbach, and Jin J. Choi, J. Appl. Phys. **72**, 1221 (1992).
[10] C. S. Kou, S. H. Chen, L. R. Barnett, H. Y. Chen, and K. R. Chu, Phys. Rev. Lett. **70**, 924 (1993).
[11] M. T. Walter, R. M. Gilgenbach, P. R. Menge, and T. A. Spencer, IEEE Trans. Plasma Sci. **22**, 578 (1994).
[12] W. C. Gauss, K. E. Kreisher, R. J. Temkin, M. Caplon, and B. Kulke, in *Conference Digest of the Fourteenth International Conference on Infrared Millimeter Waves*, edited by R. J. Temkin (IEEE, New York, 1989), p. 369.
[13] T. A. Spencer, C. E. Davis, K. J. Hendricks, F. J. Agee, and R. M. Gilgenbach, IEEE Trans. Plasma Sci. **24**, 630 (1996).
[14] M. T. Walter, R. M. Gilgenbach, J. W. Luginsland, J. M. Hochman, J. I. Rintamaki, R. L. Jaynes, Y. Y. Lau, and T. A. Spencer, IEEE Trans. Plasma Sci. **24**, 636 (1996).
[15] A. W. Fliflet, Int. J. Electron. **16**, 1049 (1986).
[16] Q. S. Wang, C. S. Kou, D. B. McDermott, A. T. Lin, K. R. Chu, and N. C. Luhmann, Jr., IEEE Trans. Plasma Sci. **20**, 163 (1992).
[17] J. W. Gewartowski and H. A. Watson, *Principle of Electron Tube* (Van Nostrand, Princeton, 1965), p. 183.
[18] T. H. Kho and A. T. Lin, Phys. Rev. A **40**, 2486 (1989).